View Online / Journal Homepage / Table of Contents for this issue
Dynamic Article Links

Nanoscale

Cite this: *Nanoscale*, 2011, **3**, 2854

www.rsc.org/nanoscale

COMMUNICATION

Formation of monolayer and few-layer hexagonal boron nitride nanosheets *via* surface segregation†

Mingsheng Xu,*[ab] Daisuke Fujita,[c] Hongzheng Chen[a] and Nobutaka Hanagata[de]

Received 19th March 2011, Accepted 22nd April 2011
DOI: 10.1039/c1nr10294j

We report that few-layer hexagonal boron nitride (h-BN) nanosheets can be produced by using a surface segregation method. The formation of h-BN sheets is *via* an intermediate boron–nitrogen buffer layer. Our results suggest that surface segregation of boron and nitrogen from a solid source is an alternative approach to tailoring synthesis of h-BN sheets for potential applications such as in graphene electronics.

Few-layer two-dimensional (2D) boron nitride (BN) sheets are drawing a great deal of attention owing to graphene technologies and their superb chemical stability and intrinsic insulation. Use of hexagonal boron nitride (h-BN) thin film as a thin top dielectric layer to gate graphene and as an inert flat substrate for graphene transistors could significantly improve device performance.[1] Boron nitride shows a similarly structured carbon lattice while consisting of an equal number of boron and nitrogen atoms. Hexagonal BN is comprised of alternating boron and nitrogen atoms in a honeycomb arrangement consisting of sp^2-bonded 2D layers. Hexagonal BN powder is traditionally used as a lubricant. Due to its good electrical insulation property, h-BN has also been applied as a charge-leakage barrier layer for electronic equipment. It also shows far-ultraviolet light emission, possibly due to its direct wide band gap (about 5.9 eV).[2] BN nanosheets have been fabricated by mechanical exfoliation,[3,4] liquid phase sonication,[5–10] and chemical vapor deposition on various metal substrates.[11–26] Surface segregation by heat treatment of doped bulk samples to synthesize graphene[27–29] and h-BN[30–36] dates back several decades, and now carbon segregation has become one of the most important approaches for producing extended single-layer graphene.[37]

Previously, BN thin films have been synthesized *via* surface segregation, that is, vacuum thermal treatment of iron–chromium–nickel (Fe–Cr–Ni) alloys doped with boron (B) and nitrogen (N). As a result, its inert effect in ultrahigh vacuum applications was demonstrated.[33] As characterized by Auger electron spectroscopy (AES) and electron diffraction, the synthesized BN films had a hexagonal structure with a preferred orientation, and they tended to cover a substrate surface with their (001) basal plane.[32–36] However, few high-resolution electron images of such synthesized h-BN films have been reported.[33] Furthermore, the phenomenon involved in boron and nitrogen segregation is not so clear.[32,34–36] Some reports showed that nitrogen segregation precedes boron segregation, that is, nitrogen is segregated first and traps boron to form epitaxial h-BN films,[32,34] whereas others showed that nitrogen and boron precipitate together on the surface and then epitaxially form h-BN films or that boron and nitrogen precipitate directly as epitaxial h-BN films.[36] Previous work was focused on the growth of thick h-BN films for an inert ultrahigh vacuum application. In the present paper, we report formation of monolayer and few-layer h-BN nanosheets by segregation of boron and nitrogen atoms from a bulk Fe–Cr–Ni alloy doped with B and N. Our high-resolution electron microscope images show that triangular h-BN nanosheets can be formed in a layer-by-layer manner, and the growth is independent of the crystallographic orientation of the polycrystalline Fe–Cr–Ni alloy. A boron–nitrogen (B–N) buffer layer co-existing with sulfur (S) atoms is observed, and transformation of the buffer layer into h-BN layers is proposed as the growth mechanism. The synthesized h-BN sheets exhibit high oxidation resistance of the alloy in air. These results suggest that surface segregation of boron and nitrogen from a solid source is an alternative approach to tailoring synthesis of h-BN sheets with potential for fine control over number of layers, shape, and structural quality.

Fig. 1 shows a typical scanning electron microscope (SEM) image of the h-BN sheets produced under the conditions described in the Experimental section. Monolayer and few-layer h-BN nanosheets were formed at the same sample (see ESI, Fig. S1†), suggesting the possibility to control the size and the number of h-BN sheets by further optimization of the synthesis process conditions, such as treatment temperature and time, cooling rate, and dopant concentrations. It is clear that individual h-BN domains can be grown either

[a]*State Key Laboratory of Silicon Materials, MOE Key Laboratory of Macromolecule Synthesis and Functionalization, and Department of Polymer Science and Engineering, Zhejiang University, Hangzhou, 310027, P. R. China. E-mail: msxu@zju.edu.cn*
[b]*International Center for Young Scientists, National Institute for Materials Science, 1-2-1 Sengen, Tsukuba, Ibaraki, 305-0047, Japan*
[c]*Advanced Key Technology Research Division, National Institute for Materials Science, National Institute for Materials Science, 1-2-1 Sengen, Tsukuba, Ibaraki, 305-0047, Japan*
[d]*Interdisciplinary Laboratory for Nanoscale Science and Technology, National Institute for Materials Science, 1-2-1 Sengen, Tsukuba, Ibaraki, 305-0047, Japan*
[e]*Graduate School of Life Science, Hokkaido University, Sapporo, Japan*

† Electronic supplementary information (ESI) available: Determination of the thickness of h-BN nanosheets, SEM images of h-BN sheets, AES spectra of h-BN as a function of sputtering time, SEM images obtained after sputtering with different sputtering times, and atomic concentration of h-BN sample after being sputtered for 1.9 min. See DOI: 10.1039/c1nr10294j

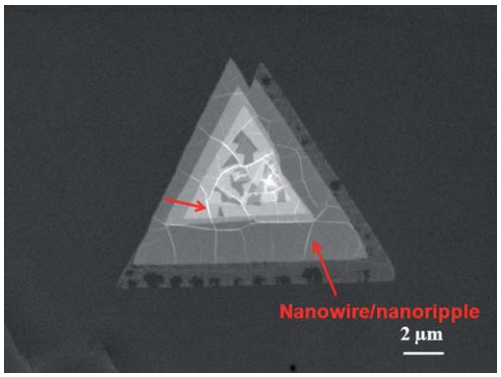

Fig. 1 Typical SEM image of h-BN nanosheets synthesized by surface segregation from Fe–Cr–Ni alloy doped with boron and nitrogen.

across various substrate domains or on a single substrate domain (see ESI, Fig. S1†), indicating the grain boundary is not the only channel for nitrogen and boron segregations. Furthermore, the growth of h-BN layers can exactly follow the steps of the substrate. These features are significant from the viewpoint of industrial applications, in particular, the requirement of seamless coating. In addition, BN nanoscale wires or ripples can continuously grow over different layers, in or on a layer without a preferable growth direction (Fig. 1 and see ESI, Fig. S1†).

AES spectroscopy was used to characterize the h-BN sheets. As shown in Fig. 2, the line shapes, *i.e.*, the green and blue curves, of B (KLL) (Fig. 2b) and N (KLL) (Fig. 2c) AES spectra resemble those given in previous reports on h-BN films,[32–34] suggesting h-BN sheets were successfully synthesized. However, the shapes of the red curves (Fig. 2b and c) do not appear like the characteristics of the h-BN layer. It is thus assumed that this layer is a buffer or intermediate B–N layer, as discussed later. An inelastic attenuation model[38,39] was used to estimate the thickness of the h-BN sheets by using an Fe (LMM) Auger transition with an electron inelastic mean free path of 1.2 nm for iron at 703 eV.[40] The estimated h-BN sheet thicknesses are 0.31, 0.65, and 0.91 nm, corresponding to the buffer layer, mono- and bi-layer BN stacks (Fig. 2a), respectively. We also used Raman spectroscopy to identify our synthesized sample as h-BN (Fig. 2d). The Raman spectra were acquired from the edge to the center points of one BN domain, which corresponds to the increase of the peak intensity. The peak position (1367 cm^{-1}) associated with the E_{2g} phonon mode and analogous to the G peak in graphene and shape is identical to the Raman feature of the mechanically exfoliated h-BN sheets.[41] Despite the change in peak intensity, it is difficult to exactly determine the number of the h-BN layers because of the poor spatial resolution of the optical microscope system.

Using electron diffraction techniques, most of the previous studies suggested epitaxial growth of h-BN on Fe–Cr–Ni,[34,36] with the basal plane (001) of h-BN covering the substrate surfaces: $(0001)_{h\text{-}BN}||(111)_{fcc\ Fe}$. Previous results suggested that surfaces of different crystallographic orientations can behave differently as sites for solute segregation in iron-based alloy systems.[42] We used electron backscatter diffraction (EBSD) to investigate the effect of the crystallographic orientation of the substrate on the formation of h-BN sheets. As shown in Fig. 3, the Fe–Cr–Ni substrate consists of varying crystalline domains with different orientations and sizes. Corresponding to the SEM image (Fig. 3a) and the image quality (Fig. 3b), the EBSD map (Fig. 3c) suggests that the crystallographic orientation of the substrate has no obvious influence on the formation of the h-BN sheets. However, the stacking of individual h-BN layers is highly oriented in a layer-by-layer manner. Although the quality of grown h-BN sheets needs further evaluation, the present results imply that h-BN layers can be easily synthesized on a polycrystalline Fe–Cr–Ni substrate.

To shed light on the segregation mechanism for forming h-BN layers, AES spectra, correlated with high-resolution SEM images and AES element mapping, were used to investigate surface segregations of sulfur, boron, nitrogen, iron, chromium, nickel, and other elements. As seen in Fig. 2e and f, the atomic concentration ratio between the B

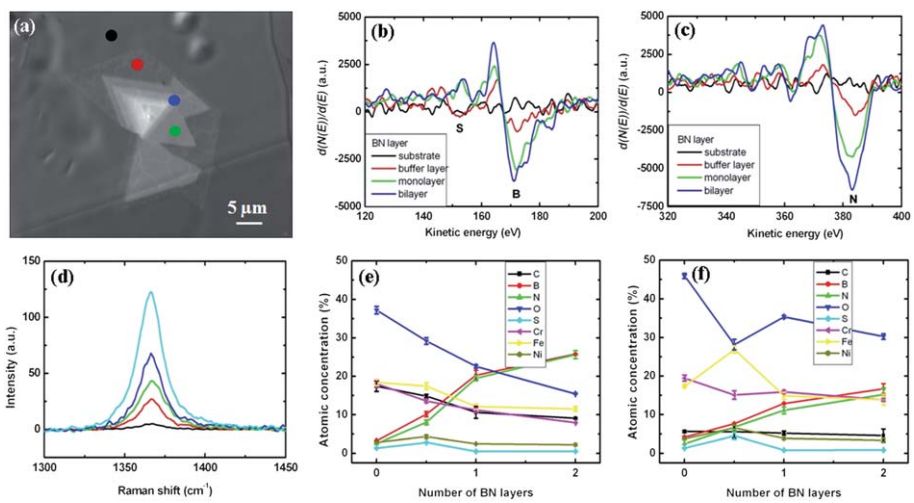

Fig. 2 Characterizations of h-BN nanosheets. (a) SEM images. The coloured points correspond to the colored curves in (b) and (c), showing where the AES spectra were obtained, and indicate substrate, buffer layer, monolayer h-BN, and bilayer h-BN regions. (b) B (KLL) spectra. (c) N (KLL) spectra. (d) Raman spectra of h-BN nanosheets on Fe–Cr–Ni substrate. The five spectra with increase of the peak intensity are obtained at the locations from the edge to the center points of one BN domain, respectively. (e) Elemental evolution without sputtering. 0.5 shown in the *x*-axis corresponds to the BN buff layer. (f) Elemental evolution after sputtering of 0.4 min. 0.5 shown in the *x*-axis corresponds to the BN buff layer.

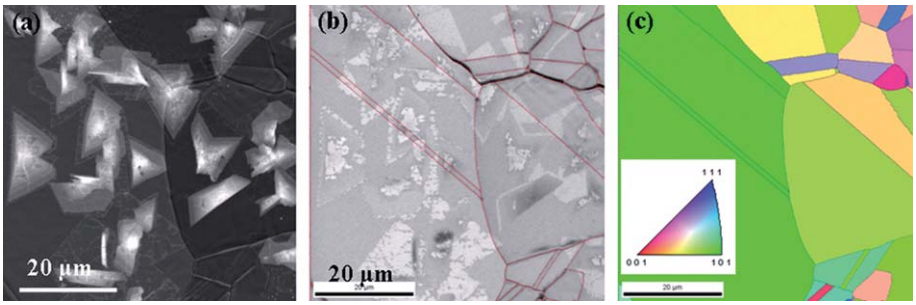

Fig. 3 Electron backscatter diffraction (EBSD) characterization of the effect of crystallographic orientation of the substrate on the formation of h-BN sheets. (a) SEM image. (b) Image quality. (c) EBSD pattern. Inverse pole $\langle h\ k\ l \rangle$ map plus grain boundaries in the sample direction of [RD TD ND] = [001], indicating that Fe–Cr–Ni grains are in various orientations. The inset shows crystal direction.

and the N determined from the mono- and bi-layer h-BN covering regions, as well as from the substrate surface, is equal to one. Whereas the atomic concentration of B obtained from the B–N buffer layer region is about 113.7% of that of N. Note that the bulk concentration of N in the Fe–Cr–Ni is much higher than that of B (see the Experimental section). This small difference between the atomic concentrations of B and N at the buffer layer region might suggest that boron and nitrogen were not simultaneously segregated. Furthermore, the atomic concentration of Cr is about 202.4% that of N. The decrease in the Cr concentration with the presence of the B–N buffer layer and varying number of the h-BN layers is believed to be due to Auger electron attenuation. This confirms the full B–N buffer layer has a different structure and different composition from those of the mono- and bi-layer h-BN. Together with the line shapes of the N (KLL) and Cr (LMM), this result also suggests metastable chromium nitrides do not form.[43] This observation is different from previous models[34,36] that were based on surface concentrations of B, N, Cr, and other elements only, without spatial correlation of the AES spectra to the location of non-homogenous h-BN films. Note that the heat treatment of our sample was different from that used in previous experiments. Despite this difference, our observation sounds reasonable if the different diffusion coefficients of boron and nitrogen in iron are considered. For example, diffusion coefficients of boron and nitrogen at 720 °C are estimated to be about 3×10^{-8} cm^2 s^{-1} and 1×10^{-9} cm^2 s^{-1}, respectively.[34] These studies suggest that not only the bulk concentrations of boron and nitrogen atoms[35] but also heat treatment influences the formation of h-BN layers.

The elemental mapping (Fig. 4) indicates stronger signals for the S and Ni atoms in the regions covered with the B–N buffer layer as compared to the surrounding regions, *i.e.*, the substrate and the h-BN regions. The variation of the S and Ni concentrations in these regions (Fig. 2e and f, and see ESI, Fig. S2 and S3†) cannot be simply explained by the attenuation effect of the Auger electrons. However, the sulfur atom showed different segregation behavior from the nickel atom. We observe much stronger sulfur signal at the substrate and the B–N buffer layer regions than that at the h-BN covering regions (Fig. 2 and 4). And the S concentration at the B–N buffer region is about three times that at the substrate region, suggesting that S atoms reside in the B–N buffer layer, but not in the h-BN layers, different from previous observation.[36] The disappearance of S in the h-BN and

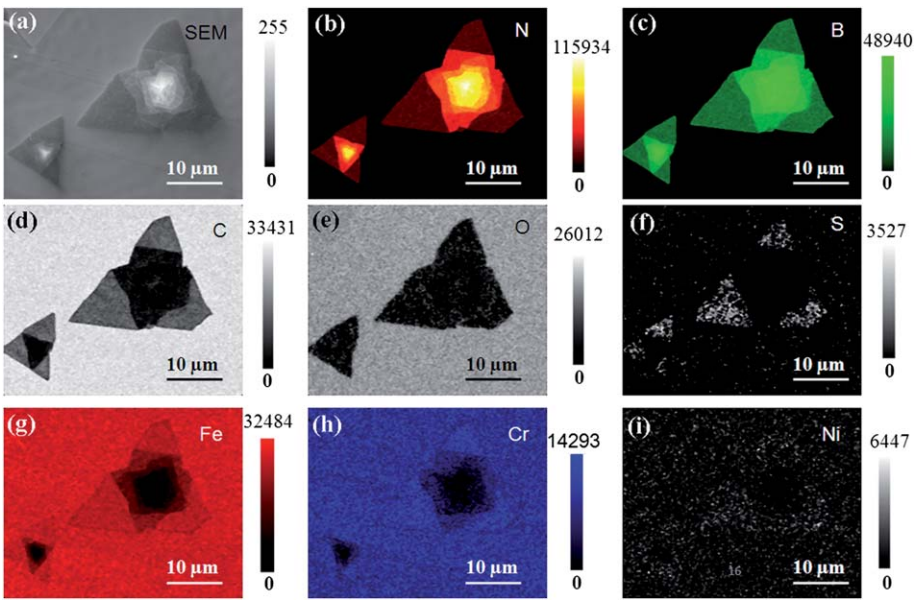

Fig. 4 Auger elemental mapping acquired at the non-sputtered surface. (a) SEM image showing where the Auger maps were obtained. (b) N (KLL) map. (c) B (KLL) map. (d) C (KLL) map. (e) O (KLL) map. (f) S (KLL) map. (g) Fe (LMM) map. (h) Cr (LMM) map. (i) Ni (LMM) map.

at its covering region is believed to result from its dispelling after the formation of h-BN layers[36] because of high stability of h-BN. In the case of nickel, its concentration at the region covered with the B–N buffer layer is about twice that of the other regions for the non-sputtered surface (Fig. 2e) and the surface after sputtering for 0.4 min (Fig. 2f). By contrast, after sputtering for totally 1.9 min, the Ni concentration at the B–N buffer layer location is about 90% of that at other regions (Fig. S4†). These results suggest that Ni atoms might also be present in the B–N buffer layer or enriched just underneath it. The nickel enrichment was reported to be coupled with the precipitation of boron.[36] The oxygen (O) signal is mostly originated from the air exposure and thus oxides were formed. Examination of the distribution of the O (KLL) signal (Fig. 4e), we find that the oxygen could diffuse into the h-BN sheets from edges and grain boundaries, suggesting that high-quality h-BN sheets could have high oxidation resistance and h-BN layers can be used as passivation layer for blockage of diffusion and resistance of oxidation.

On the basis of the above analysis, we propose a new model for the mechanism of surface precipitation of h-BN with segregated boron and nitrogen atoms from the iron alloy (Fig. 5). In the first stage, an intermediate B–N layer forms, in which surface active sulfur atoms competitively present. In the second stage, the intermediate B–N layers transform to h-BN monolayer that simultaneously dispels S atoms away from it, thereby a new intermediate B–N buffer layer forms. The third stage is the continuous crystal growth of h-BN at the intermediate B–N layer/alloy interface in a layer-by-layer manner and in each plane. The segregation picture shows discrepancy from previously proposed models.[34,36] It is concluded that understanding of the segregation process will be helpful to tailor synthesis of high-quality h-BN sheets by the present surface segregation method.

We have demonstrated that the h-BN layers *via* an intermediate B–N buffer layer mixed with sulfur atoms were formed by surface segregation of boron and nitrogen from an iron–chromium–nickel alloy. Moreover, a new segregation model for synthesis of h-BN nanosheets was proposed. This surface segregation offers a simple and cheap pathway for mass production of mono- or few-layer h-BN films on metals or alloys containing trace amounts of boron and nitrogen atoms. Similar to production of graphene films with fine control over the crystalline structure and number of layers, this segregation approach may hold the potential for achieving high-quality h-BN layers with precise numbers of h-BN layers by optimizing boron and nitrogen contents in the bulk sample and heating program.

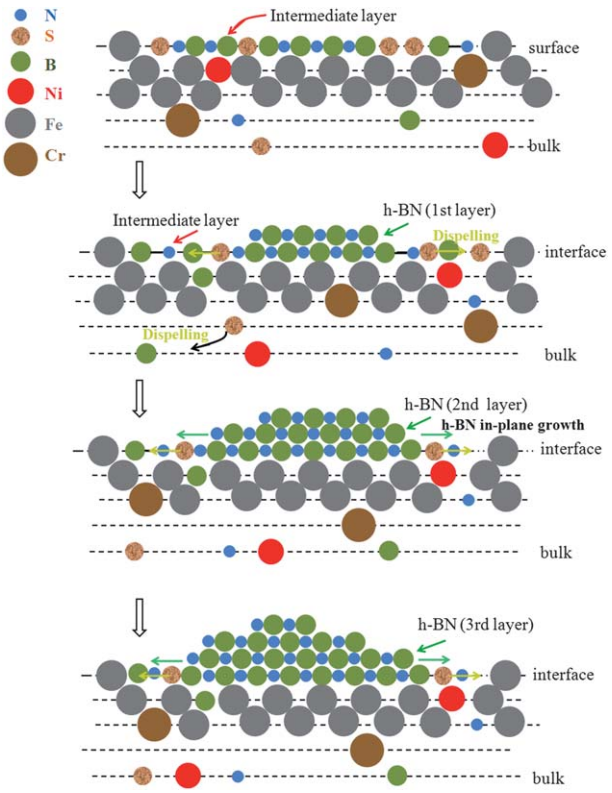

Fig. 5 Proposed model for the mechanism of surface precipitation of h-BN. In the first stage, an intermediate B–N layer, mixed with sulfur atoms, is formed. In the second stage, h-BN monolayer is formed by transformation of the B–N buffer layer, and S atoms are dispelled from the h-BN region. In the third stage, the second h-BN layer is formed underneath the first h-BN layer. h-BN film grows in a layer-by-layer manner and expands in each layer. In the intermediate or buffer layer, there is competition between nucleation of BN and existence of sulfur atoms. Once h-BN is formed, S atoms can be expelled from the h-BN.

Experimental section

Segregation growth of h-BN layers

The h-BN sheets were grown by heat treatment of a iron (67 atomic %)–chromium (18.5 atomic%)–nickel (12.4 atomic%) alloy doped with boron and nitrogen at concentrations of 0.05 and 0.6 atomic%, respectively. The alloy also contained traces of sulfur (0.002 atomic %), carbon (0.046 atomic%), molybdenum (1.4 atomic%), manganese (0.8 atomic%), and other impurities.[34] The iron–chromium–nickel alloy with boron and nitrogen dopants was firstly electropolished to minimize surface roughness and then degreased by ultrasonic cleaning in acetone. To grow h-BN layers under ultrahigh vacuum, the specimen was heated to 1000 °C within 5 min and kept at that temperature for 5 min. After that, the specimen was cooled by turning off the power supply. After the preparation, the sample was exposed to ambient air and transferred for characterization.

Scanning Auger electron spectroscopy (AES)

AES measurements were performed simultaneously with scanning electron microscopy (SEM) at room temperature with a scanning Auger electron spectroscope (ULVAC-PHI model SAM650) with a cylindrical-mirror analyzer. The take-off angle of the instrument was 42°. SEM images were acquired with a primary electron beam of 10 kV. To subtract the background from the direct Auger spectrum, differential energy spectra were used. Differential d$N(E)$/dE Auger spectra were obtained by numerical derivation of the direct $N(E)$-integrated Auger data displaying an absolute scale with counts/second units by a universal Savitzky–Golay differential filter using five points.

Scanning electron microscopy (SEM) and electron backscatter diffraction (EBSD)

SEM image and EBSD analysis of the crystallographic orientation of the iron–chromium–nickel grains with h-BN layers were carried out using a JSM-7001F field-emission scanning electron microscope with an accelerating voltage of 1 to 10 kV.

Raman spectroscopy

Raman spectra were recorded with a RAMAN-11 system (Nanophoton Corp., Japan), which illuminates a line-shaped area on the sample with a line-shaped laser beam. Raman scattering light from the line-shaped area on the sample was simultaneously detected by a parallel detection system. The scattering signal was dispersed with a Czerny-Turner type spectrometer ($f = 500$ mm, the focal length of the spectrometer) and detected with an electrically cooled charge-coupled device (CCD) detector (400 × 1340 pixels). The excitation source was a 532 nm laser with a power setting <1.0 mW to avoid laser-induced damage. The lateral resolution was about 350 nm focused by a ×100 optical lens (numerical aperture of 0.9), and the spectral resolution was about 1.6 cm^{-1}. From a Raman map, Raman spectrum at each pixel point can be collected and analyzed.

Acknowledgements

This work was supported by the National Natural Science Foundation of China (No. 51011130028, 50990063 and 50973095), by Zhejiang Provincial Natural Science Foundation of China (R4110030), and by Nanotechnology Innovation Center of National Institute for Materials Science (NIMS), Japan. We thank H. Gao for assistance of EBSD measurement.

References

1 C. R. Dean, A. F. Young, I. Meric, C. Lee, L. Wang, S. Sorgenfrei, K. Watanabe, T. Taniguchi, P. Kim, K. L. Shepard and J. Hone, *Nat. Nanotechnol.*, 2010, **5**, 722.
2 K. Watanabe, T. Taniguchi, T. Niiyama, K. Miya and M. Taniguchi, *Nat. Photonics*, 2009, **3**, 591.
3 D. Pacile, J. C. Meyer, C. O. Girit and A. Zettl, *Appl. Phys. Lett.*, 2008, **82**, 133107.
4 C. Lee, Q. Y. Li, W. Kalb, X. Z. Liu, H. Berger, R. W. Carpick and J. Jone, *Science*, 2010, **328**, 76.
5 A. Nag, K. Raidongia, K. P. S. S. Hemnram, R. Datta, U. V. Waghmare and C. N. R. Rao, *ACS Nano*, 2010, **4**, 1539.
6 W. Q. Han, L. Wu, Y. Zhu, K. Watanabe and T. Taniguchi, *Appl. Phys. Lett.*, 2008, **93**, 223103.
7 C. Zhi, Y. Bando, C. Tang, H. Kuwahara and D. Golberg, *Adv. Mater.*, 2009, **21**, 2889.
8 J. H. Warner, M. H. Rummeli, A. Bachmatiuk and B. Nuchner, *ACS Nano*, 2010, **4**, 1299.
9 J. N. Coleman, M. Lotya, A. O'Neill, S. D. Bergin, P. J. King, U. Khan, K. Young, A. Gaucher, S. De, R. J. Smith, I. V. Shvets, S. K. Arora, G. Stanton, H. Y. Kim, K. Lee, G. T. Kim, G. S. Duesberg, T. Hallam, J. J. Boland, J. J. Wang, J. F. Donegan, J. C. Grunlan, G. Moriarty, A. Shmeliov, R. J. Nicholls, J. M. Perkins, E. M. Grieveson, K. Theuwissen, D. W. McComb, P. D. Nellist and V. Nicolosi, *Science*, 2011, **331**, 568.
10 Y. Lin, T. V. Williams, T. B. Xu, W. Cao, H. E. Elsayed-Ali and J. W. Connell, *J. Phys. Chem. C*, 2011, **115**, 2679.
11 H. O. Pierson, *J. Compos. Mater.*, 1975, **9**, 228.
12 A. C. Adams, *J. Electrochem. Soc.*, 1981, **128**, 1378.
13 G. Constant and R. Feurer, *J. Less-Common Met.*, 1981, **82**, 113.
14 A. S. Rozenberg, Y. A. Sinenko and N. V. Chukanov, *J. Mater. Sci.*, 1993, **28**, 5528.
15 S. Middleman, *Mater. Sci. Eng., A*, 1993, **163**, 135.
16 A. Nagashima, N. Tejima, Y. Gamou, T. Kawai and C. Oshima, *Phys. Rev. B: Condens. Matter Mater. Phys.*, 1995, **51**, 4606.
17 R. M. Desrosiers, D. W. Greve and A. J. Gellman, *Surf. Sci.*, 1997, **382**, 35.
18 W. Auwarter, M. Muntwiler, J. Osterwalder and T. Greber, *Surf. Sci.*, 2003, **545**, L735.
19 M. Corso, W. Auwarter, M. Muntwiler, A. Tamai, T. Greber and J. Osterwalder, *Science*, 2004, **303**, 217.
20 W. Auwarter, H. U. Suter, H. Sachdev and T. Greber, *Chem. Mater.*, 2004, **16**, 343.
21 F. Muller, K. Stowe and H. Sachdev, *Chem. Mater.*, 2005, **17**, 3464.
22 A. B. Preobrajenski, A. S. Vinogradov and N. Martensson, *Surf. Sci.*, 2005, **582**, 21.
23 M. Morscher, M. Corso, T. Greber and J. Osterwalder, *Surf. Sci.*, 2006, **600**, 3280.
24 E. Cavar, R. Westerstrom, A. Mikkelsen, E. Lundgren, A. S. Vinogradov, M. L. Ng, A. B. Preobrajenski, A. A. Zakharov and N. Martensson, *Surf. Sci.*, 2008, **602**, 1722.
25 S. Li, L. J. Ci, H. Lu, P. B. Sorokin, C. H. Jin, J. Ni, A. G. Kvashnin, D. G. Kvashnin, J. Lou, B. I. Yakobson and P. M. Ajayan, *Nano Lett.*, 2010, **10**, 3209.
26 Y. M. Shi, C. Hamsen, X. T. Jia, K. K. Kim, A. Reina, M. Hofmann, A. L. Hsu, K. Zhang, H. N. Li, Z. Y. Juang, M. S. Dresselhaus, L. J. Li and J. Kong, *Nano Lett.*, 2010, **10**, 4134.
27 J. C. Shelton, H. R. Patil and J. M. Blakely, *Surf. Sci.*, 1974, **43**, 493.
28 D. Fujita and K. Yoshihara, *J. Vac. Sci. Technol., A*, 1994, **12**, 2134.
29 J. H. Gao, D. Fujita, M. S. Xu, K. Onishi and S. Miyamoto, *ACS Nano*, 2010, **4**, 1026.
30 R. H. Stulen and R. Bastasz, *J. Vac. Sci. Technol. (N. Y., NY, U. S.)*, 1979, **16**, 940.
31 K. Yoshihara, M. Tosa and K. Nii, *J. Vac. Sci. Technol., A*, 1985, **3**, 1804.
32 D. Fujita, K. Yoshihara and T. Homma, *J. Japan Inst. Metals*, 1992, **4**, 406.
33 D. Fujita and T. Homma, *J. Vac. Sci. Technol., A*, 1988, **6**, 230.
34 D. Fujita and T. Homma, *Thin Solid Films*, 1989, **181**, 267.
35 Y. Minami, A. Tohyama and T. Yamada, *J. Vac. Sci. Technol., A*, 1989, **7**, 1585.
36 C. A. Long and H. J. Grabke, *Appl. Surf. Sci.*, 1992, **59**, 207.
37 M. S. Xu, D. Fujita, S. Sagisaka, E. Watanabe and N. Hanagata, *ACS Nano*, 2011, **5**, 1522.
38 M. S. Xu, D. Fujita, J. H. Gao and N. Hanagata, *ACS Nano*, 2010, **4**, 2937.
39 *Practical Surface Analysis: Auger and X-ray Photoelectron Spectroscopy*, ed. D. Briggs and M. P. Seah, John Wiley & Sons, New York, 1990.
40 S. Tanuma, C. J. Powell and D. R. Penn, *Surf. Interface Anal.*, 1991, **17**, 911.
41 R. V. Gorbachev, I. Riaz, R. R. Nair, R. Jalil, L. Britnell, B. D. Belle, E. W. Hill, K. S. Novoselov, K. Watanabe, T. Taniguchi, A. K. Geim and P. Blake, *Small*, 2011, **7**, 465–468.
42 H. J. Brabke, V. Leroy and H. Viefhaus, *ISIJ Int.*, 1995, **35**, 95.
43 C. Uebing, H. Viefhaus and H. J. Grabke, *Appl. Surf. Sci.*, 1988, **32**, 363.

